Electrochemical and theoretical evaluation of thiocarbohydrazide as a brass (60/40) corrosion inhibitor in 3% NaCl solution and effect of temperature on this process

H. Bouayadi,[1,2] M. Damej,[1,2,3] A. Molhi,[3] Z. Lakbaibi,[4] M. Benmessaoud[3] and M. Cherkaoui[1,2]

[1]Organic Chemistry, Catalysis and Environment Laboratory at Ibn Tofail University, Faculty of Science, BP 133, 14000 Kenitra, Morocco
[2]National School of Chemistry, University Campus, B.P 241, Kenitra, 14000, Morocco
[3]Environment, Materials and Sustainable Development Team-CERNE2D, High School of Technology, Mohammed V University in Rabat, Morocco
[4]Laboratory of Molecular Chemistry, Materials and environment (LCME2), Multidisciplinary Faculty Nador, Mohamed first University, Oujda, BP 300 Selouane 62700, Nador, Morocco
**E-mail: Bouayadihamid@gmail.com*

Abstract

This work presents an in-depth analysis of the inhibitory effects of thiocarbohydrazide (TCH) on the corrosion behavior of brass (60Cu-40Zn) in 3% NaCl solution similar to seawater using electrochemical measurements (electrochemical impedance spectroscopy and potentiodynamic polarization), scanning electron microscopy (SEM) and quantum chemistry calculations (DFT, MC, MD). The study's intent is to evaluate the possibility of using this molecule as an inhibitor for brass. The experimental results indicate that TCH has a very good corrosion inhibiting property toward brass in 3% NaCl. The calculated inhibition efficiency was 92.81% for a maximum concentration studied, namely, 1 mM TCH. Acceptable correlations were obtained between the inhibition efficiency and the calculated quantum chemical parameters. Studies of the temperature effect confirmed that the adsorption of TCH to the surface of brass is consistent with the Langmuir adsorption isotherm in the temperature range used. In addition, we found that this compound is characterized by a chemisorption process. Thermodynamic variables and activation energy values were determined and interpreted. The density functional theory (DFT) calculations, electrostatic potential surface (EPS), Monte Carlo (MC) and radial distribution function (RDF) simulations were achieved to obtain more insights about the adsorption mechanism of TCH towards the 60Cu-40Zn brass alloy (BA) surfaces. Moreover, the standard free adsorption energies ΔG^0_{ads} obtained suggest strong adsorption of the inhibitor to the metal surface. The presence of TCH on active sites on the brass surface was confirmed experimentally by SEM analysis.

Received: December 27, 2021. Published: September 13, 2022 doi: 10.17675/2305-6894-2022-11-3-25

Keywords: *thiocarbohydrazide, brass, electrochemistry, corrosion, adsorption, DFT–MC.*

1. Introduction

Copper and its alloys are very important materials. They exhibit remarkable corrosion resistance in neutral aggressive media, high formability, as well as high electrical and thermal conductivity [1–7]. They are commonly used in condensers and heat exchangers in power plants [2, 6]. Recently, copper alloys, especially brass, are widely used in water distribution systems for the manufacture of fasteners, tubing and in shipbuilding [2, 3]. However, its corrosion depends on the environment it is immersed in and on other factors such as the presence of corrosive ions such as chloride ions and sulphide ions present in solution or the presence of oxygen [8, 9]. The selective corrosion of brass is basically a process of dezincification which occurs due to the difference in nobility between Cu and Zn (Cu is nobler than Zn). Therefore, Zn will corrode first and to form a porous structure rich in Cu with decreased mechanical properties [4]. Generally, a corrosive attack can be mitigated by using inhibitors or controlling the pH, so research shows that compounds that comprise nitrogen, sulfur and oxygen atoms are effective inhibitors for brass corrosion. These complex compounds act by forming a protective film on the brass surface [1].

In this investigation, a concentration of 1 mM TCH was used, which is at times employed in industry [8]. Moreover, 3% by weight is an ordinary concentration of NaCl used in corrosion inhibitor studies, which in turn enables a highly corrosive environment to clearly show the effective behavior of TCH against brass corrosion.

In this article, the phenomenon of brass corrosion was studied in a corrosive solution (3% NaCl). The aim was to examine the influence of different TCH concentrations and temperature on the corrosion behavior using electrochemical impedance spectroscopy (EIS), potentiodynamic polarization, and open circuit potential (OCP) measurements to elucidate the phenomenon of brass corrosion. The adsorption behavior of TCH onto BA surfaces was highlightted using DFT, ESP, MC and RDF calculations.

2. Experimental

2.1. Inhibitor tested

The compound tested as a corrosion inhibitor is thiocarbohydrazide as a technical-commercial inhibitor of “FLOCKA” grade. The chemical structure of this compound is as shown in figure 1.

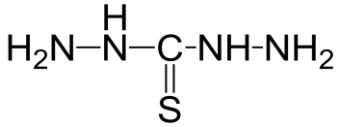

Figure 1. Structure of the inhibitor tested.

2.2. Sample composition

The brass electrode used in these tests has an elemental composition of (% by weight): 60.61% Cu, 39.19% Zn, 0.12% Al and 0.08% Si and a contact area of 0.78 cm^2. To ensure proper electrical connection for electrochemical testing, it was soldered to pure copper wire and coated with epoxy resin. Before each test, the electrodes were manually polished with emery paper, rinsed with double-distilled water, and dried.

2.3. Solution

The NaCl solution (3% by weight) was made by dissolving sodium chloride in distilled water.

2.4. Electrochemical techniques

The electrochemical measurements were carried out in a conventional three-electrode cell (Potentiostat model PGZ101): a saturated calomel electrode (SCE) was the reference electrode; a graphite rod was the counter electrode, and brass was the working electrode. The electrochemical workstation was connected to a computer and equipped with Volta master software (4). EIS measurements were made at a series of frequencies from 100 kHz to 10 mHz.

After one hour of immersion, an EIS measurement was carried out. Then the polarization plots were recorded at a scanning rate of 1 mV/s and in the range from 1000 mV to 400 mV.

2.5. SEM/EDX

The brass samples from this study were immersed in the aggressive 3% NaCl solution in the absence and in the presence of the TCH inhibitor and at the maximum concentration studied (1 mM TCH) for 24 hours. Then, the surface was studied by the Quanta 200 FEI Company scanning electron microscopy coupled to EDS.

2.6. Theoretical procedure

The optimized structure of TCH was calculated using the DFT method [9] with the 6-311G++ (2d,2p) basis [10] and the B3LYP functional [11] utilizing Gaussian 09 software [12]. As for BA surfaces, their optimization was done employing the Gaussian 09 suite integrated in Material studio Biovia version 8.0 with the same basis and functional as indicated above. The most nucleophilic centers and the most electrophilic centers for all TCH atoms were determined in terms of Mulliken atomic spin density (MASD) analysis [13] using nucleophilic P^- and electrophilic P^+ Parr indices. Additionally, the reactive areas of the TCH inhibitor studied were estimated from the ESP analysis. The MC simulation interface (TCH–BA) was applied in 3% NaCl solution ($10Na^+$, $10Cl^-$, $100H_2O$) using the adsorption locator module and the COMPASS II force field integrated to the Materials

Studio version 8 software [14]. The analysis RDF was performed for the most favorable interface using Forcite calculation code.

3. Results and Discussion

3.1. Concentration effect

3.1.1. Polarization curve

The corrosion behavior of brass in 3% NaCl was analyzed by potentiodynamic polarization curves. As expected, all cathodic and anodic polarization plots were recorded after 1 hour of immersion at the free corrosion potential. The impact of TCH at various concentrations was examined. The values of the associated electrochemical parameters are displayed in table 1.

The cathodic and anodic curves of the Cu-40Zn alloy in 3% NaCl solution in the absence and in the presence of TCH are shown in Figure 2. Analysis of the figure and the table reveals the following points.

In the cathodic domain: Corrosion current density (i_{corr}) decreased with increasing TCH concentration which caused the corrosion potential to shift towards negative values. The curve shows a current diffusion plateau, indicating the influence of mass transport in the cathodic process. The reduction of oxygen observed in the cathodic domain is a mixed process (diffusion/activation) at the corrosion potential [6]. From Table 1, it is noted that the corrosion current density varies from 10.20 μA·cm^{-2} without the inhibitor to 0.94 μA·cm^{-2} at 1 mM TCH concentration.

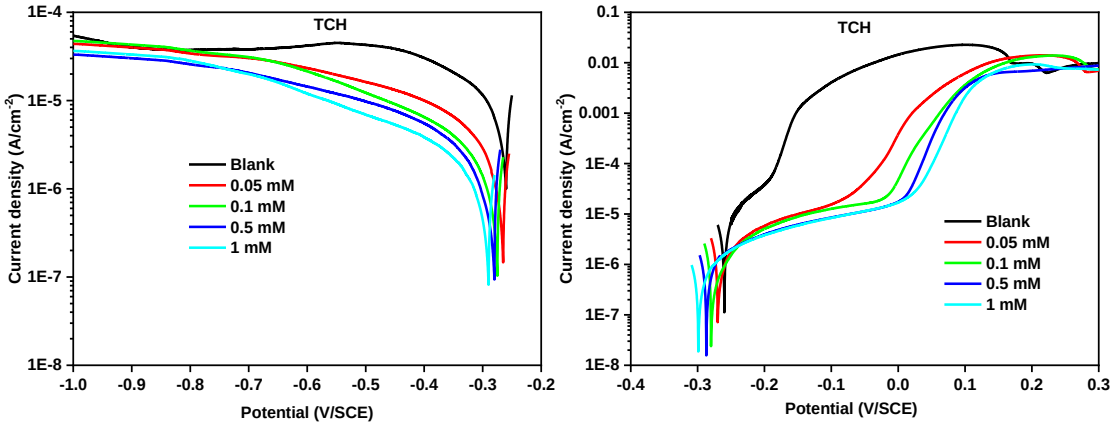

Figure 2. Polarization curves in the cathodic and anodic domain for the samples of brass in NaCl 3% at TCH concentrations ranging from 0 to 1 mM.

In the anodic domain: In the presence of TCH, the anodic curves shifted towards negative potentials with a passive zone between –0.2 and 0 V/SCE at the various concentrations of TCH. As the concentration of TCH inhibitor increased, the performance of the passivation film gradually increased. Addition of a maximum concentration studied

of the TCH inhibitor (1 mM) caused a maximum decrease in i_{corr} to 0.79 μA·cm^{-2}. At the highest concentration of TCH, the inhibition efficiency reached a maximum value of 91.51%.

Table 1. Electrochemical parameters from polarization measurements on 60Cu-40Zn alloy at various TCH concentrations.

[TCH]	Cathodic branch			Anodic branch			*IE* %
	E_{corr} (mV/SCE)	i_{corr} (μA/cm^2)	b_c (mV/dec)	E_{corr} (mV/SCE)	i_{corr} (μA/cm^2)	b_a (mV/dec)	
0 mM	–260	10.20	–296	–259	9.30	92	–
0.05 mM	–264	2.07	–264	–270	1.36	116	85.37
0.1 mM	–275	1.52	–255	–280	1.21	124	86.99
0.5 mM	–280	1.27	–230	–287	1.04	135	88.82
1 mM	–290	0.94	–184	–299	0.79	136	91.51

3.1.2. Electrochemical impedance spectroscopy

The corrosion mechanism of brass in 3% NaCl solution similar to seawater in the presence of TCH was studied by electrochemical impedance spectroscopy technique at room temperature.

Figure 3 below shows the Nyquist and Bode plots of the Cu-40Zn alloy in aggressive 3% NaCl solution without and with different concentrations of the TCH inhibitor after 1 hour of stabilization time and Table 2 contains parameters such as double layer capacitance (C_{dl}), charge transfer resistance (R_{ct}), and inhibition efficiency (*IE*). As a reminder, the *IE* of TCH was calculated by relation (1):

$$IE\% = \frac{R_{p(inh)} - R_p}{R_{p(inh)}} \cdot 100 \quad (1)$$

where R_p and $R_{p(inh)}$ are the polarization resistance without and with the inhibitor, respectively.

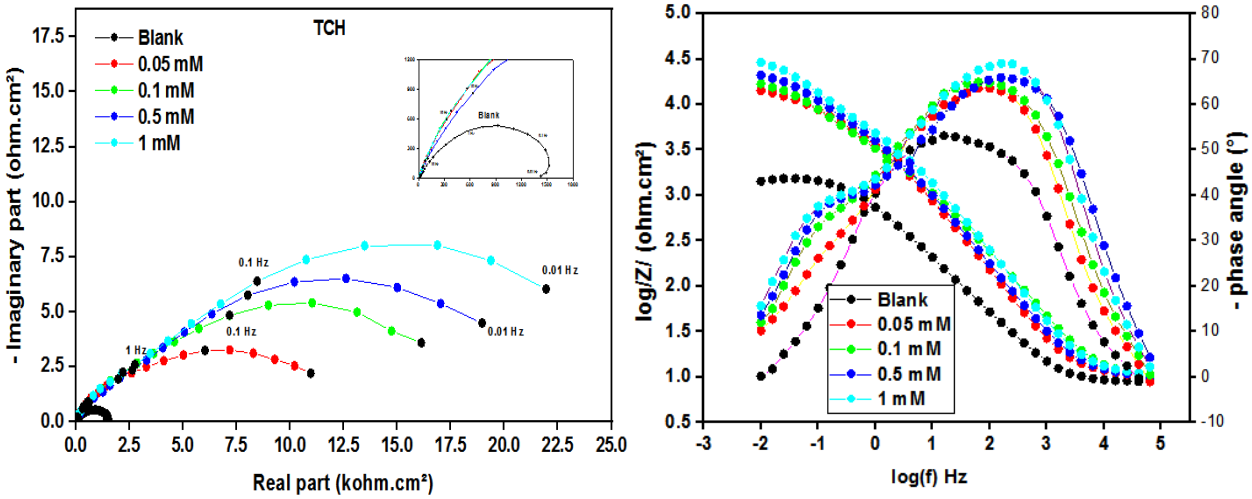

Figure 3. Electrochemical impedance plots generated at the interface 60Cu-40Zn/3% NaCl at different concentrations of TCH.

Table 2. Electrochemical impedance parameters of 60Cu-40Zn alloy in aggressive 3% NaCl solution without and with different concentrations of the TCH inhibitor.

[TCH]	R_f (kΩ·cm²)	C_f (μF·cm⁻²)	R_{ct} (kΩ·cm²)	C_{dl} (μF·cm⁻²)	n_{dl}	*IE*, %
0 mM	–	–	1.42	112.10	0.67	–
0.05 mM	3.10	2.05	8.82	45.11	0.72	83.90
0.1 mM	5.22	1.21	13.58	29.30	0.78	89.54
0.5 mM	4.93	1.29	17.61	22.59	0.75	91.94
1 mM	6.24	1.02	19.76	20.13	0.81	92.81

The plots show a single capacitive loop in the absence of TCH inhibitor and two capacitive loops in its presence [15]. The diameter of the low-frequency capacitive loop increases from 1.42 kΩ·cm² in the absence of the inhibitor to 19.76 kΩ·cm² in the presence of 1 mM TCH. The values of R_{ct} and C_{dl} change from 8.85 kΩ·cm² 45.11 μF·cm⁻² to 19.76 kΩ·cm² and 20.13 μF·cm⁻², respectively. These variations confirm that the presence of TCH retards the corrosion rate and the film of products created on the surface of the brass electrode becomes more protective in the presence of 1 mM TCH. While R_{ct} values increased, in contrast, C_{dl} values decreased with an increase in the inhibitor concentration. The change in C_{dl} may be due either to an increase in the thickness of the electrical double layer or a decrease in the local dielectric constant or to both [2, 6, 16, 17]. The maximum inhibition efficiency value was 92.81% at 1 mM TCH concentration.

The corresponding Bode plots of the impedance spectrum of different samples are also shown in Figure 3. First, the log |*Z*| plots of the samples are close to each other, and a single

time constant is detected at TCH concentrations between 0.05 mM and 1 mM. At TCH concentrations greater than 0.1 mM, a second time constant appears: this behavior is observed in the presence of two different contributions. The first one localized at high frequencies is associated with the film and the second one, with the charge transfer at the interface. As the TCH concentration increased, the traces shifted upward and produced a gap, showing that the corrosion resistance capacity increased with the TCH concentration [4, 18].

This confirms that the TCH inhibitor retards the corrosion rate and that the protective film formed on the surface of the brass electrode becomes increasingly dense with increasing TCH concentration [13]. The equivalent circuit is displayed in Figure 4 to understand the inhibition mechanisms that take place at the metal/electrolyte interface.

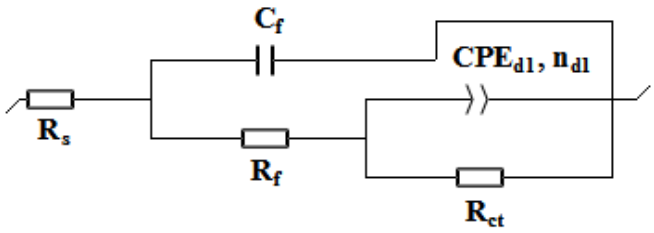

Figure 4. Equivalent circuit used to fit the EIS data of brass electrode in 3% NaCl without and with different concentrations of TCH.

This equivalent circuit has two-stroke constants in figure 4, in addition to the resistance of the solution *R*s. The charge transfer resistance (R_{ct}) is connected in parallel to the constant phase element (CPE_{dl}, n_{dl}), which represents the low frequency time constant. The second high frequency time constant is formed by the film capacitance (C_f) in parallel to the film resistance (R_f) [8, 9]. The values of C_f and the double layer capacitance decrease as the concentration of TCH increases, which is evident as the film becomes denser at the surface of the brass electrode [14].

3.2. *Adsorption isotherm*

The adsorption mechanism of a compound, e.g., an inhibitor, is controlled by several factors such as the chemical structure of the inhibitor, existence of molecular charge, metal charge, and aggressive solution. To shed light on the adsorption interaction between the brass surface and the TCH inhibitor, the adsorption isotherm was examined [15]. The adsorption isotherm found for TCH is plotted in Figure 5.

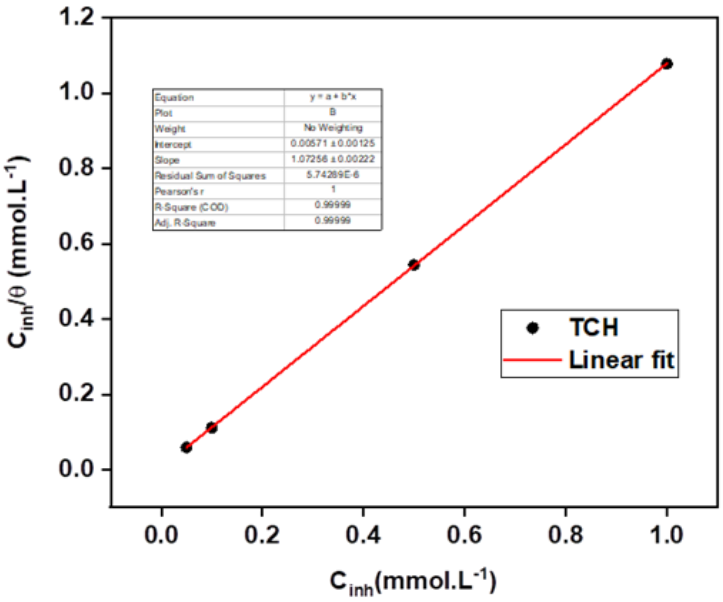

Figure 5. Langmuir adsorption diagram of TCH on brass in 3%NaCl solution. The Langmuir adsorption isotherm has a linear regression coefficient (R^2) close to 1, which provides the best description of the adsorption behavior of TCH on the brass surface.

The R^2 is equal to 0.9999 indicating that the adsorbed molecules occupy only one site [1]. The standard free adsorption energies can be calculated using Equation 2:

$$-\Delta G^0_{\text{ads}} = \ln K - \ln\left(\frac{1}{55.55}\right) \cdot R \cdot T \tag{2}$$

where R is the universal gas constant; T is the temperature.

Table 3. The parameters of the Langmuir isotherm with the TCH inhibitor

Inhibitor	K **(mol^{-1}·L)**	R^2	ΔG^0_{ads} **(kJ·mol^{-1})**
TCH	175.13	0.9999	–22.76

The standard free adsorption energies obtained suggests strong adsorption of TCH inhibitor to the metal surface. The value of the ΔG^0_{ads} of adsorption was negative (–22.76 kJ /mol^{-1}), which suggests that the adsorption of TCH at the level of the brass surface is a spontaneous process and that it is physicochemical adsorption [5, 15].

3.3. Temperature effect

Temperature studies provide insight into the inhibitory adsorption mechanism by calculating the activation energies in the absence and presence of the TCH inhibitor with the intention

of analyzing the behavior of this inhibitor at higher temperatures. Consequently, several researchers confirm that temperature accelerates the kinetics of chemical reactions, such as chemical adsorption and desorption [13, 16]. The polarization curves and the corrosion parameters (E_{corr} *vs*. SCE), i_{corr} and *IE*) in the absence and in the presence of a maximum inhibitor concentration studied (1 mM TCH) were studied in the temperature range from 293 K up to 323 K. The results obtained from the polarization and corrosion parameters at different temperatures are presented in Figure 6 and Table 4.

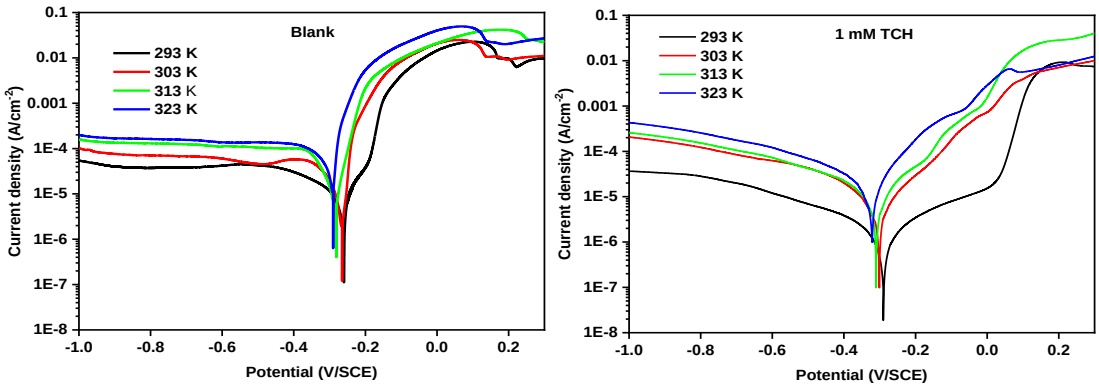

Figure 6. The impact of temperature on the polarization plots of the brass electrode in 3% NaCl solution without an inhibitor and at the maximum inhibitor concentration studied (1mM TCH).

In accordance with the polarization plots and Table 4, we observed the disappearance of the passive zone in the anodic domain in the presence of TCH when the temperature was greater than or equal to 303 K. Thus, i_{corr} increases and *IE* % decreases with the rise in temperature while E_{corr} remains almost invariable. This is interpreted by the physical adsorption process of the protective layer (the film formed).

Table 4. Corrosion parameters of a brass electrode in 3% NaCl solution without an inhibitor and in the presence of 1 mM of TCH at different temperatures.

***T* (K)**	**E_{corr} (mV/SCE)**	**i_{corr} (μA/cm^2)**	***IE* %**
	Blank		
293	–259	10.30	–
303	–265	25.12	–
313	–282	53.45	–
323	–292	78.52	–

***T* (K)**	***E*corr (mV/SCE)**	***i*corr (μA/cm²)**	***IE* %**
	1 mM TCH		
293	–290	0.85	91.52
303	–300	3.93	85.06
313	–308	10.67	80.04
323	–317	19.84	74.73

As described by relations (4) and (5), the Arrhenius equations allow the calculation of the standard activation energy (E_a), the enthalpy (ΔH_a) and entropy (ΔS_a).

$$i_{corr} = A\exp\left(-\frac{E_a}{RT}\right) \quad (4)$$

where A is the frequency factor, R is the gas constant, and T is the absolute temperature.

$$i_{corr} = \frac{R\cdot T}{N\cdot h}\exp\left(\frac{\Delta S_a}{R}\right)\exp\left(\frac{\Delta H_a}{R\cdot T}\right) \quad (5)$$

where N is the Avogadro number and h is the Plank constant.

The Arrhenius graphs of ln i_{corr}/T *vs.* $1/T$ and ln i_{corr} *vs.* $1/T$ for a brass electrode in 3% NaCl solution in the presence and in the absence of the inhibitor are plotted in Figure 6. The intersection of equation (5) with the ordinate is equal to $\ln\left(\frac{R}{N\cdot h}\right)+\frac{\Delta S_a}{R}$ and the slopes of the linear part of the curves are equal to $\left(-\frac{k\cdot E_a}{R}\right)$ and $\left(\frac{-\Delta H_a}{R}\right)$, respectively. From them, the values of E_a, ΔH_a and ΔS_a were precisely determined and presented in Table 5 [17].

Table 5. The values of ΔH_a and ΔS_a and activation energy for a brass electrode in 3% NaCl solution in the absence and in the presence of 1 mM TCH.

Inhibitor	***E*a (kJ/mol)**	**Δ*H*a (kJ/mol)**	**Δ*S*a (J/mol·K)**
Blank	53.37	50.83	–321.25
TCH	81.38	84.16	–329.81

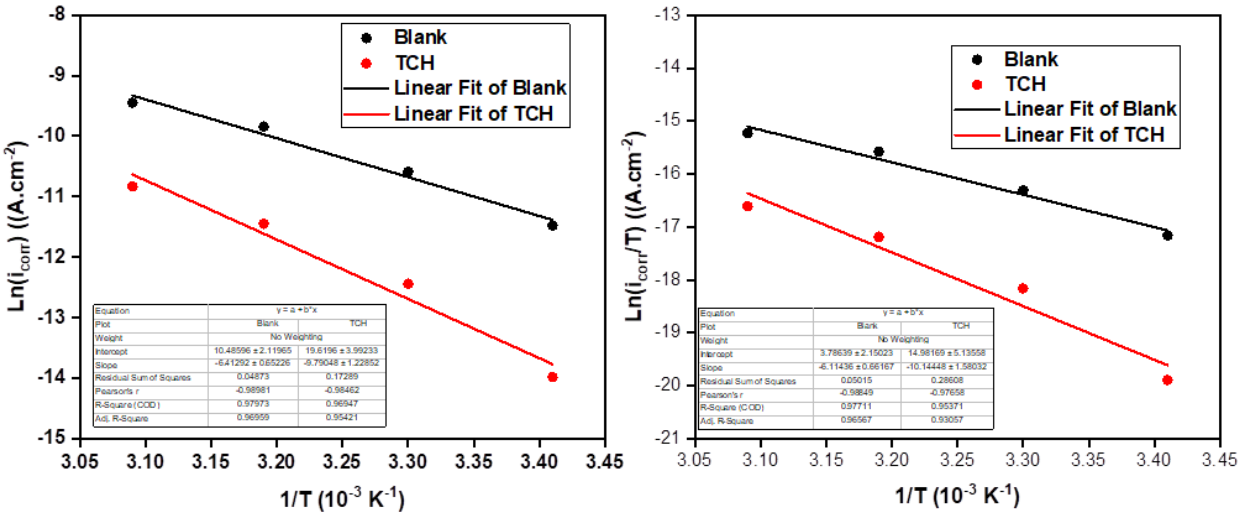

Figure 7. Arrhenius plots for a brass electrode in 3% NaCl solution in the presence and in the absence of the inhibitor.

The ΔH_a values are positive in the absence and in the presence of TCH, suggesting the endothermic nature of the brass dissolution mechanism [17]. Studies of the effect of temperature on standard activation energy are characterized by chemisorption when E_a decreases and by physical adsorption in the reverse case [7]. In our research, the addition of the maximum TCH concentration studied results in $E_a = 81.38$ kJ/mol, which was higher than that of the metal without inhibitor (53.37 kJ/mol); this is manifested in the case of chemisorption, in other words, the interaction process involves covalent bonds.

3.4. Surface analysis SEM/EDX

The analysis of the prepared samples was carried out after immersion in the corrosive medium (3% NaCl) for 24 hours with and without the addition of 1 mM TCH; the results obtained are shown in Figures 8 and 9.

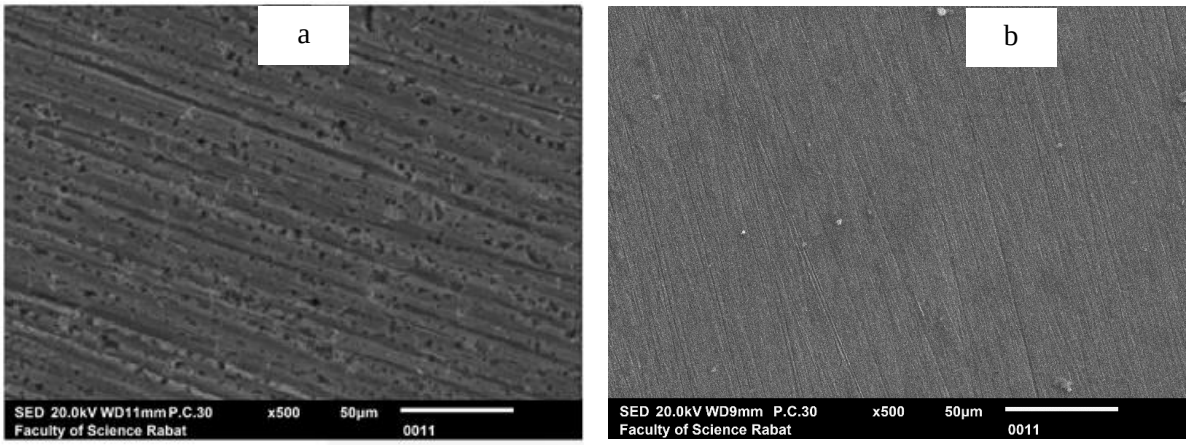

Figure 8. SEM micrographs of the surface of brass 60Cu-40Zn in 3% NaCl solution in the absence (a) (blank) and in the presence of 1 mM TCH (b).

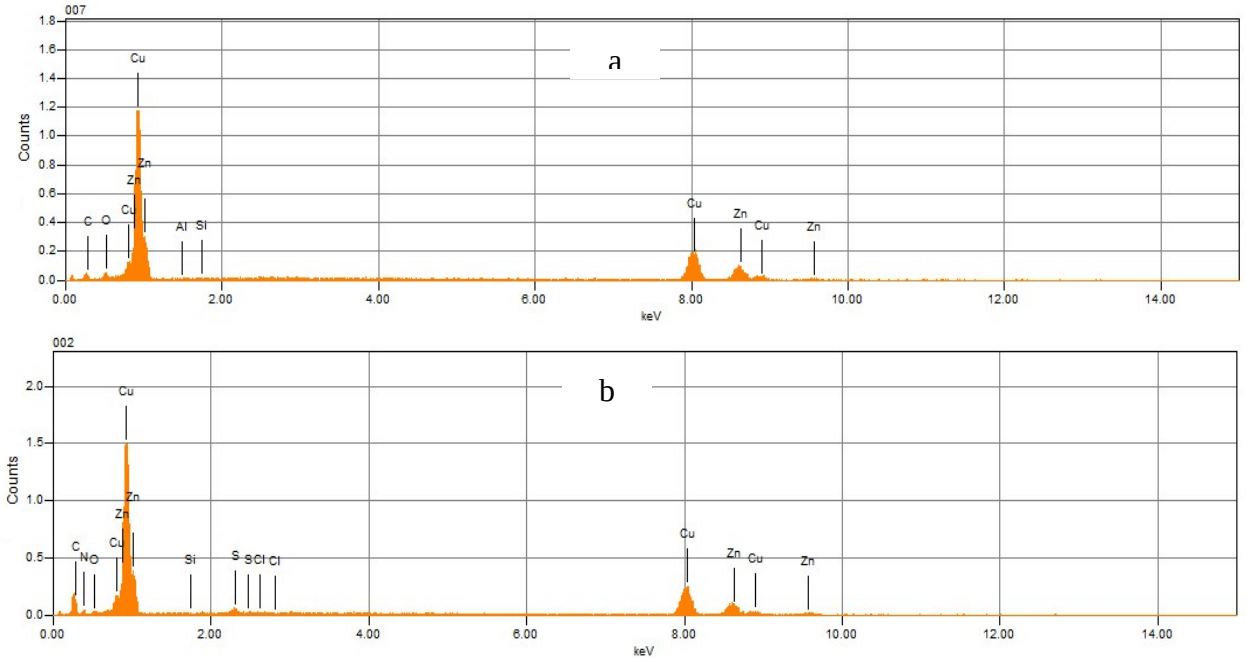

Figure 9. EDX analysis of the surface of brass 60Cu-40Zn after immersion for 24 hours in 3% NaCl solution in the absence (a) and in the presence of 1 mM THC (b).

In 3% NaCl solution (Figure 8a), the surface of brass 60Cu-40Zn underwent a severe corrosion attack and the porous layer of corrosion products was present. Addition of TCH (Figure 8b) was accompanied by the formation of a protective film, which can be explained by the adhesion of the inhibitor to the surface, which suppresses the corrosion process.

EDX analysis (Figure 9a) shows the presence of peaks characteristic of certain elements constituting brass. In the presence of TCH (Figure 9b), EDX spectra show additional lines such as carbon, oxygen and sulfur indicating the presence of an inhibitor film on the metal surface [5, 23, 24].

3.5. MASD and ESP study

The TCH molecule was optimized and the results are shown in Figure 10.

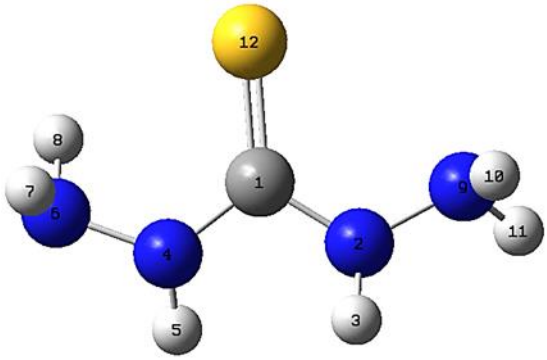

Figure 10. Optimized structure of TCH.

The optimization calculations were confirmed by the presence of zero negative frequency in the *z*-matrix. Nucleophilic P^- and electrophilic P^+ Parr indices were calculated for the principal atoms of TCH (Table 6).

Table 6. Nucleophilic P^- and electrophilic P^+ Parr indices calculated for all TCH atoms. For atom numbering, see Figure 1.

		TCH	
No.	**Atoms**	P^-	P^+
1C	Carbon	NNS	NES
2N	Nitrogen	NNS	NES
3H	Hydrogen	NNS	**1.151**
4N	Nitrogen	NNS	0.058
5H	Hydrogen	NNS	**0.467**
6N	Nitrogen	0.059	NES
7H	Hydrogen	NNS	0.122
8H	Hydrogen	NNS	0.019
9N	Nitrogen	NNS	NES
10H	Hydrogen	NNS	0.362
11H	Hydrogen	NNS	0.509
12S	Sulphur	0.926	NES

NNS: no nucleophilic site; NES: no electrophilic site. Table 6 shows that the TCH molecule has both nucleophilic and electrophilic reactive centres simultaneously (higher values of P^- and P^+). This certainly determines the donating and anti-donating properties of TCH. The higher and lower values of P^- are attributed to the sulphury atom (S12) and nitrogen atom (N6), respectively. The higher values of P^+ are attributed to the hydrogen atoms (H3, H5, H7, H10 and H11), while the low values are found at a nitrogen atom (N4) and a hydrogen atom (H8). Therefore, it is noticed that TCH comprises atoms that are not nucleophilic nor electrophilic reactive (negative values of P^- and P^+). As a result, we can draw important information that TCH has a tendency to donate electrons to the unoccupied d orbital of the metal to form coordinate covalent bonds and can also accept free electrons from the metal by using their anti-bonding orbital to form feed-back bonds.

To gain further insights about the reactivity of the studied structure (TCH) towards BA (*i.e.*, brass alloy: 60Cu-40Zn) surface, the ESP calculations are used to know the electron rich (ER) and electron poor (EP) regions over TCH structure that are responsible for the interaction with the metal. Figure 11 exposes the ESP fitting scheme of TCH structure where the red color signifies a strong negative electrostatic potential distribution (SNEP); yellow

(moderately negative MNEP); blue (strong positive SPEP); green (moderately positive MPEP) and cyan (low positive LPEP) [25].

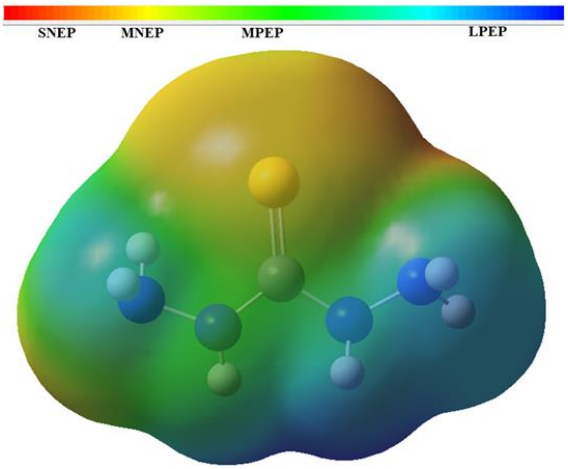

Figure 11. ESP map of TCH structure.

As displayed in Figure 11, it can be seen that the sulphonyl group (–S=O) in TCH is the most susceptible region for the nucleophilic attacks (red color); while the amino groups (–NH_2 and –NH–) presents a strong region (blue color) and a weak electrophilic region (green color), respectively. This result suggests that TCH has a high tendency to donate and receive electrons when it interacts is with the BA surface.

3.6. MC and RDF study

The MC simulation for the characteristic surfaces of BA referred to in literature such as (111), (200), (220), (311) and (222) with cell parameters of $a = b = 11.780\ Å$ and $\alpha = \beta = \gamma = 90°$, containing a vacuum layer of 20 *Å* along the C-axis. Figure 12 exhibits the equilibrium adsorption of the studied interfaces between TCH inhibitor and BA surface. To estimate the *strongest* adsorption related to the interfaces under study, some energetic parameters were calculated: the total energy (E_T) reports the global energy for the system, this parameter is calculated by optimizing the whole system; therefore, the adsorption energy (E_{ads}) which displays the energy required when the relaxed TCH inhibitor is adsorbed on the surface, is generally known to estimate the forte and mechanism of adsorption; another term of energy is the desorption energy $dE_{ads}/dNi(TCH)$ that reflects the necessary energy on which one entity of TCH is removed to the system that contains TCH, solution and BA surface (Table 6) [26–30]. Therefore, the adsorption behavior (*i.e.*, chemisorption, physisorption or both) related to the studied systems was evaluated from RDF analysis using Forcite calculation code for the most favorable interface. This method was suggested as a powerful tool to estimate the bond lengths in the adsorption process. The appearance of peaks with lengths smaller than 3.5 *Å* is considered an indication of small bonds, and is correlated with chemisorption, while physical adsorption behavior is associated with peaks greater than 3.5 *Å* [26–29].

According to Table 7, we noticed that E_T and E_{ads} energies related to the adsorption of TCH on BA surfaces increased in the follow order: BA(111) <BA(200) <BA(220) <BA(222) <BA(311). This ordering suggests that the most stable and stronger adsorption is related to the TCH–BA(111) interface. This observation is strengthened by comparison of the desorption energy (dE_{ads}/dNi) values that show that the TCH–BA(111) interface has the higher value of dE_{ads}/dNi –44.305 kcal/mol). Further, we observed that the calculated adsorption energies are all negative, indicating clearly that the studied adsorption can be spontaneously shaped and thus, the TCH inhibitor has qualitatively an adsorption capability to interact with the BA surface. As RDF analysis shows (Figure 13), we note that the adsorption type of TCH onto BA(111) is chemisorption (peaks with distances < 3.5 *Å*) and physisorption (peaks with distances > 3.5 *Å*); this means that the TCH inhibitor coordinates to BA(111) surface through both chemical and physical interactions.

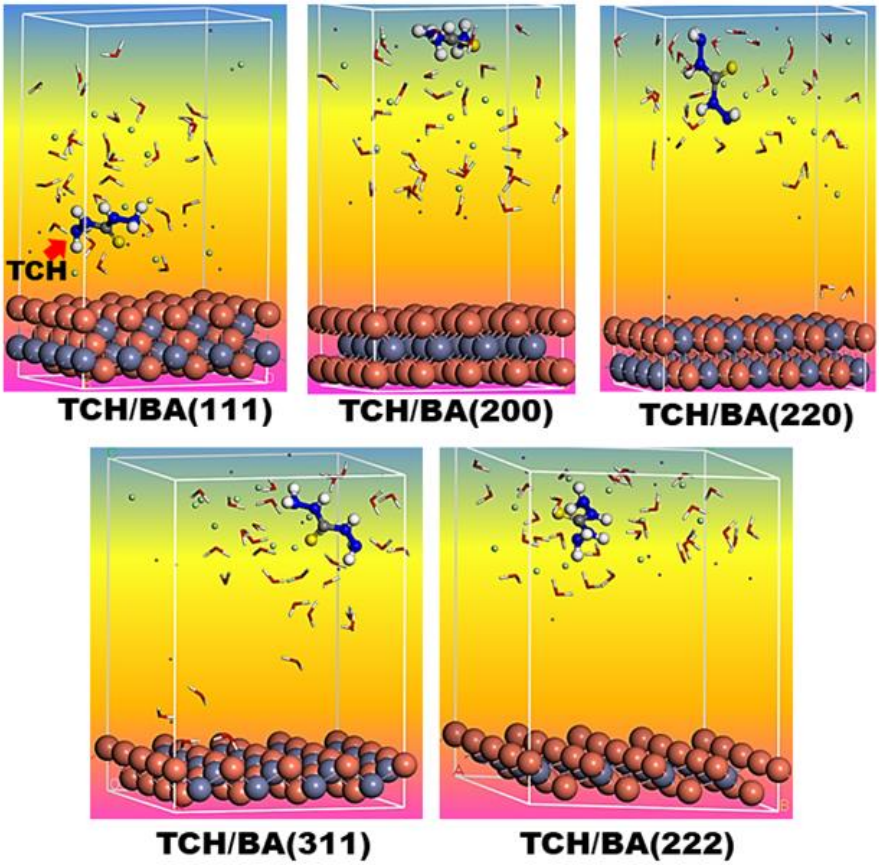

Figure 12. The stable adsorption configurations of TCH inhibitor on BA surfaces in 3% NaCl solution ($10Na^+$, $10Cl^-$, $100H_2O$) at 298.15 K and 1 atm.

Table 7. Total energy E_T, adsorption energy E_{ads}, and necessary energy to remove one TCH molecule from the surface dE_{ads}/dNi in 3% NaCl solution ($10Na^+$, $10Cl^-$, $100H_2O$) at 298.15 K and 1 atm.

	E_T (kcal·mol^{-1})	E_{ads} (kcal·mol^{-1})	dE_{ads}/dNi (TCH) (kcal·mol^{-1})
TCH/BA(111)	–132.097	–282.897	–44.305
TCH/BA(200)	–71.222	–158.957	–63.1627
TCH/BA(220)	–66.005	–153.740	–66.643
TCH/BA(311)	–40.222	–127.959	–71.854
TCH/BA(222)	–62.396	–150.131	–66.843

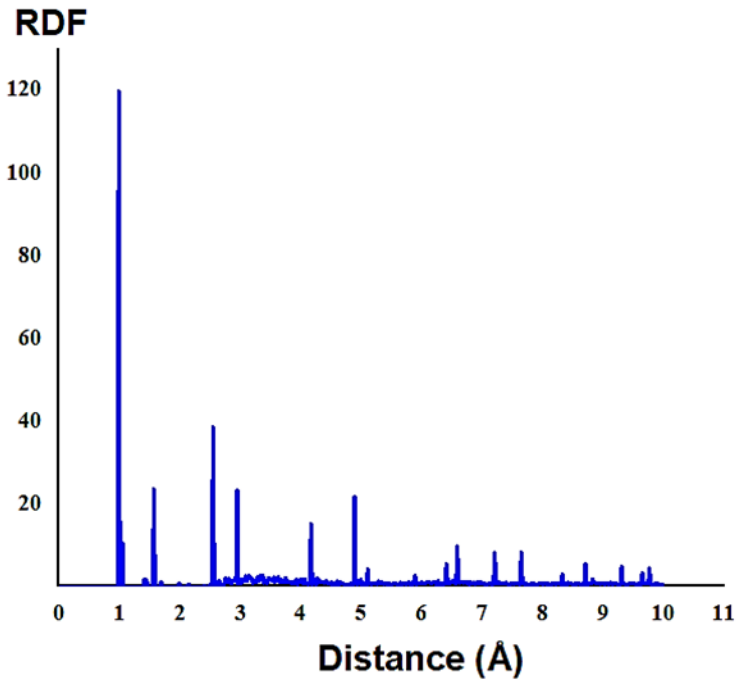

Figure 13. Radial distribution function analysis associated to the TCH–solution–BA(111) interface.

Conclusion

After completing the experiments and analyzing the data, the following conclusions were drawn:

- TCH exhibits very good inhibitory properties for brass in 3% NaCl solution similar to seawater, which are controlled by a mixed inhibitor type. Its maximum efficiency reached 92.81% for a maximum concentration studied of 1 mM TCH in 3% NaCl solution.
- The corrosion current density decreased with increasing TCH concentration and the charge transfer resistance values also increased, but on the other hand, the double layer capacitance decreased, which confirms that the TCH inhibitor decreases the

corrosion rate. Also, the film created on the surface of the brass electrode becomes dense and more protective in the presence of a maximum concentration studied of TCH (1 mM).

- The Langmuir adsorption isotherm provides the best description of the adsorption behavior of TCH on the brass surface. The value of the standard free adsorption energy suggests that the adsorption of TCH on the surface of brass is physical and chemical adsorption.
- Studies of the effect of temperature show a standard activation energy in the presence of 1 mM TCH (81.38 kJ/mol). It is greater than that of brass without an inhibitor (53.37 kJ/mol), which is an indication of chemisorption.
- DFT, ESP, Monte Carlo, and RDF analysis highlighted a deeper explanation of the agreement between the adsorption behavior and the inhibition ability.

References

1. M. B. Radovanović, Ž. Tasić, M. B. P. Mihajlović, A. T. Simonović and M. M. Antonijević, Electrochemical and DFT studies of brass corrosion inhibition in 3% NaCl in the presence of environmentally friendly compounds, *Sci. Rep*., 2019, **9**, no. 1, 16081. doi: 10.1038/s41598-019-52635-2
2. M. Damej, H. Benassaoui, D. Chebabe, M. Benmessaoud, H. Erramli, A. Dermaj, N. Hajjaji and A. Srhiri, Inhibition effect of 1,2,4-triazole-5-thione derivative on the corrosion of brass in 3% NaCl solution, *J. Mater. Environ. Sci*., 2016, **7**, 738–745.
3. M. Damej, D. Chebabe, M. Benmessaoud, A. Dermaj, H. Erramli, N. Hajjaji and A. Srhiri, Corrosion inhibition of brass in 3% NaCl solution by 3-methyl-1,2,4-triazol-5-thione, *Corros. Eng. Sci. Technol*., 2015, **50**, 103–107. doi: 10.1179/1743278214Y.0000000207
4. Z. Liang, K. Jiang, T. Zhang, and S. Lin, Corrosion behavior of Western Zhou Dynasty brass in a corrosive archaeological environment, *J. Alloys Compd*., 2021, **865**, 158579. doi: 10.1016/j.jallcom.2020.158579
5. M. Damej, D. Chebabe, S. Abbout, H. Erramli, A. Oubair, and N. Hajjaji, Corrosion inhibition of brass 60Cu-40Zn in 3% NaCl solution by 3-amino-1, 2, 4-triazole-5-thiol, *Heliyon*, 2020, no. 6, e04026. doi:10.1016/j.heliyon.2020.e04026
6. Z. Mountassir and A. Srhiri, Electrochemical behaviour of Cu–40Zn in 3% NaCl solution polluted by sulphides: Effect of aminotriazole, *Corros. Sci*., 2007, **49**, no. 3, 1350–1361. doi: 10.1016/j.corsci.2006.07.001
7. H. Keleş and S. Akça, The effect of Variamine Blue B on brass corrosion in NaCl solution, *Arab. J. Chem*., 2019, **12**, no. 2, 236–248. doi: 10.1016/j.arabjc.2015.02.007
8. H. Benassaoui, M. Damej, E. Benassaoui, A. Dermaj, H. Erramli, N. Hajjaji and A. Srhiri, Electrosynthesis and Characterization of Adherent Poly on B66 Bronze Electrode in Methanol, *Port. Electrochim. Acta*., 2020, **38**, 299–312. doi: 10.4152/pea.202005299

9. S. Tighadouini, S. Radi, M. El Massaoudi, Z. Lakbaibi, M. Ferbinteanu and Y. Garcia, Efficient and Environmentally Friendly Adsorbent Based on β-Ketoenol-Pyrazole-Thiophene for Heavy-Metal Ion Removal from Aquatic Medium: A Combined Experimental and Theoretical Study, *ACS Omega*, 2020, **5**, no. 28, 17324–17336. doi: 10.1021/acsomega.0c01616
10. P. C. Hariharan and J. A. Pople, The influence of polarization functions on molecular orbital hydrogenation energies, *Theor. Chim. Acta*, 1973, **28**, no. 3, 213–222. doi: 10.1007/BF00533485
11. A. Jaafar, Z. Lakbaibi, B. Adbelghani, H. Ben El Ayouchia, K. Azzaoui, M. H. Tabyaoui and S. Jodeh, Degradation of Pollutant Dye in Aqueous Solution using Fenton Reaction: A DFT Study, *G. P. Globalize Res. J. Chem*., 2018, **2**, no. 1, 9.
12. M. Damej, A. Molhi, K. Tassaoui, B. El Ibrahimi, Z. Akounach, A.A. Addi, S. El Hajjaji and M. Benmessaoud, Experimental and Theoretical Study to Understand the Adsorption Process of p-Anisidine and 4-Nitroaniline for the Dissolution of C38 Carbon Steel in 1M HCl, ChemistrySelect., 2022, **7**, e202103192. doi: 10.1002/slct.202103192
13. Z. Lakbaibi, A. Jaafar, H. Ben El Ayouchia, M. Tabyaoui and A. Boussaoud, Reactivity and mechanism of nucleophilic addition reaction of amine with alkene: A systematic DFT study, *Mediterr. J. Chem*., 2019, **8**, no. 1, 25–29. doi: 10.13171/mjc811902924zlhbea
14. M. Damej, S. Kaya, B. EL Ibrahimi, H. S. Lee, A. Molhi, G. Serdaroğlu, M. Benmessaoud, I. H. Ali, S. EL Hajjaji and H. Lgaz, The corrosion inhibition and adsorption behavior of mercaptobenzimidazole and bis-mercaptobenzimidazole on carbon steel in 1.0 M HCl: Experimental and computational insights, *Surfaces and Interfaces*., 2021, **24,** 101095. 10.1016/j.surfin.2021.101095
15. H. Fan, S. Li, Z. Zhao, H. Wang, Z. Shi and L. Zhang, Inhibition of brass corrosion in sodium chloride solutions by self-assembled silane films, *Corros. Sci*., 2011, **53**, no. 12, 4273–4281. doi: 10.1016/j.corsci.2011.08.039
16. K. Dahmani, M. Galai, M. Ouakki, M. Cherkaoui, R. Touir, S. Erkan, S.Kaya and B. El Ibrahimi, Quantum chemical and molecular dynamic simulation studies for the identification of the extracted cinnamon essential oil constituent responsible for copper corrosion inhibition in acidified 3.0 wt% NaCl medium, *Inorg. Chem. Commun*., 2021, **124**, 108409. doi: 10.1016/j.inoche.2020.108409
17. A. Molhi, R. Hsissou, M. Damej, A. Berisha, M. Bamaarouf, M. Seydou, M. Benmessaoud and S. El Hajjaji, Performance of two epoxy compounds against corrosion of C38 steel in 1 M HCl: Electrochemical, thermodynamic and theoretical assessment, *Int. J. Corros. Scale Inhib*., 2021, **10,** 812–837. doi: 10.17675/2305-6894-2021-10-2-21
18. H. Nady, N. H. Helal, M. M. El-Rabiee and W. A. Badawy, The role of Ni content on the stability of the ternary Cu-Al-Ni alloy in neutral chloride solutions, *Mater. Chem. Phys*., 2012, **134**, no. 2–3, 945–950. doi: 10.1016/j.matchemphys.2012.03.096

19. A. Chraka, I. Raissouni, N. Benseddik, S. Khayar, A. Ibn Mansour, H. Belcadi, F. Chaouket, D. Bouchta, Effect of the aging time of Ammi visnaga (L.) lam essential oil on the chemical composition and corrosion inhibition of brass in a 3% NaCl medium. Experimental and theoretical studies, *Mater. Today: Proc*., 2020, **22**, 83–88. doi: 10.1016/j.matpr.2019.08.086
20. M. J. Bahrami, S. M. A. Hosseini and P. Pilvar, Experimental and theoretical study of organic compounds as corrosion inhibitors of mild steel in sulfuric acid medium, *Corros. Sci*., 2010, **52**, no. 9, 2793–2803. doi: 10.1016/j.corsci.2010.04.024
21. A. Popova, M. Christov and A. Vasilev, Inhibitory properties of quaternary ammonium bromides of N containing heterocycles on acid corrosion of mild steel. Part I: Gravimetric and voltametric results, *Corros. Sci*., 2007, **49**, no. 8, 3276–3289. doi: 10.1016/j.corsci.2007.03.011
22. B. Ould Abdelwedoud, M. Damej, K. Tassaoui, A. Berisha, H. Tachallait, K. Bougrin, V. Mehmeti and M. Benmessaoud, Inhibition effect of N-propargyl saccharin as corrosion inhibitor of C38 steel in 1M HCl, experimental and theoretical study, *J. Mol. Liq*., 2022, **354**, 118784. doi: 10.1016/j.molliq.2022.118784
23. M. Damej, H. Benassaoui, D. Chebabe, M. Benmessaoud, H. Erramli, A. Dermaj, N. Hajjaji and A. Srhiri, Inhibition effect of 1,2,4-triazole-5-thione derivative on the corrosion of brass in 3% NaCl solution, *J. Mater. Environ. Sci*., 2016, **7**, 738–745.
24. M. Damej, M. Zouarhi, M. Doubi, M. Chellouli, H. Benassaoui and H. Erramli, Study of the protective effect of green inhibitor extracted from seeds oil of Cannabis sativa L . against corrosion of brass 60Cu-40Zn in seawater medium, *Int. J. Corros. Scale Inhib*., 2020, **9**, 1564–1579. doi: 10.17675/2305-6894-2020-9-4-24
25. M. Manssouri, Z. Lakbaibi, M. Znini, Y. E. L. Ouadi, A. Jaafar and L. Majidi, Impact of Aaronsohnia pubescens Essential Oil to Prevent Against the Corrosion of Mild Steel in 1.0 M HCl: Experimental and Computational Modeling Studies, *J. Fail. Anal. Prev*., 2020, **20**, no. 6, 1939–1953. doi: 10.1007/s11668-020-01003-8
26. M. Manssouri, M. Znini, Z. Lakbaibi, A. Ansari and Y. El Ouadi, Experimental and computational studies of perillaldehyde isolated from Ammodaucus leucotrichus essential oil as a green corrosion inhibitor for mild steel in 1.0 M HCl, *Chem. Pap*., 2021, **75**, no. 3, 1103–1114. doi: 10.1007/s11696-020-01353-5
27. A. Ansari, Z. Lakbaibi, M. Znini, M. Manssouri and A. Laghchimi, Evaluation of Corrosion Inhibition and Adsorption Behavior of 7-Isopropyl-4-methyl-4,5,6,7-tetrahydrobenzoisoxazole against Carbon Steel Corrosion in 1 M HCl. Experimental and Computational Investigations, 2020, **8**, no. 2, 16. doi: 10.22036/ABCR.2020.233677.1509
28. D. Chebabe, S. Abbout, M. Damej, A. Oubair, Z. Lakbaibi, A. Dermaj, H. Benassaoui, M. Doubi and N. Hajjaji, Electrochemical and Theoretical Study of Corrosion Inhibition on Carbon Steel in 1M HCl Medium, *J. Fail. Anal. Prev*., 2020, **20**, 1673–1683. 10.1007/s11668-020-00974-y

29. A. Jaafar, A. Darchen, S. El Hamzi, Z. Lakbaibi, A. Driouich, A. Boussaoud, A. Yaacoubi, M. El Makhfouk and M. Hachkar, Optimization of cadmium ions biosorption by fish scale from aqueous solutions using factorial design analysis and Monte Carlo simulation studies, *J. Environ. Chem. Eng*., 2021, **9**, no. 1, 104727. doi: 10.1016/j.jece.2020.104727
30. M. Damej, R. Hsissou, A. Berisha, K. Azgaou, M. Sadiku, M. Benmessaoud, N. Labjar and S. El Hajjaji, New epoxy resin as a corrosion inhibitor for the protection of carbon steel C38 in 1M HCl. experimental and theoretical studies (DFT, MC, and MD), *J. Mol. Struct*., 2022, **1254**, 132425. doi: 10.1016/j.molstruc.2022.132425

♦ ♦ ♦